A kinetic study of the plasma-etching process. II. Probe measurements of electron properties in an rf plasma-etching reactor

M. J. Kushner[a)]
Sandia National Laboratories, Division 4216, Albuquerque, New Mexico 87185

(Received 23 July 1981; accepted for publication 15 December 1981)

Electrical probe measurements made in an rf plasma-etching reactor are discussed as a function of gas mix and position in the reactor. Comparisons are made to a kinetic model for the plasma etching process. The electron density as a function of the ratio CF_4/H_2 and CF_4/O_2 was found to decrease as the fraction of CF_4 decreased, although local extrema in electron density were observed. The electron flux distribution was also found to show extrema as the gas mixture was changed. The spatial variations of electron density and temperature between the electrodes were found to be a function of electrode material.

PACS numbers: 52.25.Lp, 52.80.Pi, 82.65.Nz, 52.40.Hf

I. INTRODUCTION

Plasma etching is a process currently used in the fabrication of semiconductor devices.[1–4] In this process, an rf discharge is used to generate fluorine-bearing radicals and ions from various inorganic and organic gases. These radicals are adsorbed on the selected surface where they bond with the lattice members, desorbing as a volatile such as SiF_4, thereby etching the substrate. Despite a number of mass spectroscopic,[5–8] optical,[9–11] and theoretical investigations of the process,[12,13] the application of plasma etching to the construction of semiconductor devices is still largely an empirical art.

Plasma-etching rf discharges are very complex systems. A typical plasma-etching discharge is sustained in a parallel-plate reactor with electrodes 20–50 cm in diameter, separated by less than 10 cm. The gases used are mixtures of fluorocarbons or inorganic fluorinated gases (e.g., CF_4, C_2F_6, C_2F_4, CF_3H, SF_6) with an additive such as O_2 or H_2. The operating pressure is $\lesssim 100$ mTorr. The peak-to-peak rf voltage applied to the discharge can be many hundreds of volts. Although most of this voltage is shielded from the plasma by sheaths at the electrodes, the resulting plasma is very hot, with average electron temperatures greater than 10 eV. The parent gases are subject not only to electron-impact collisions but also gas-phase chemical and surface-initiated reactions.

There have been a number of probe studies made in rf and microwave discharges[14–19] as well as in discharges specifically for plasma etching.[20–23] The problem in plasma-etching discharges is complicated by the large parameter space that must be mapped, not only in gas composition, pressure, and electric field strength, but also in the plasma-etching reactor configuration. A variety of reactor geometries are currently in use, among these being parallel plate, barrel, and reactive ion-diode and triode arrangements.[4]

In this paper, results of a Langmuir probe study of plasma-etching discharges in a parallel-plate reactor are reported. The purpose of this study is to attempt to characterize some of the basic plasma properties of plasma-etching discharges over a parameter space not previously investigated. The dependence of electron density on gas composition and position in the reactor will be discussed. Comparisons to a kinetic model for the plasma-etching process will be made.

II. PROBE THEORY AND LIMITATIONS

Electrostatic Langmuir probes are one of the basic tools of the plasma physicist for measuring electron densities, temperatures, and energy distributions. Although Langmuir probes are mechanically simple, the theory of their use is complex and, as a result, interpretation of the results is at times difficult. Reviews of probe theory can be found in Refs. 24 and 25. The basic points will be discussed below.

Consider a probe biased to a voltage V immersed in a low-pressure plasma. The bias potential is the sum of the voltage drop between the reference electrode and the sheath boundary (V_s), and the sheath boundary and the probe (V_p). Assuming Maxwellian electrons, for $V_p < 0$ (i.e., a repulsive potential), the electron current drawn by the probe is

$$i_e = -\tfrac{1}{4} n_0 e [(8kT_e)/(\pi m_e)]^{1/2} A \exp(eV_p/kT_e), \quad (1)$$

where n_0 is the total electron density, e and m_e are the electronic charge and mass, respectively, T_e is the electron temperature, and A is the collecting area of the probe. The conditions which must be satisfied for (1) to apply are that the sheath thickness be small compared to the dimensions of the probe, and that the mean-free-path of electrons be large compared to the diameter of the probe. Differentiating the log of (1) one obtains

$$(d \ln i_e)/(dV_p) = e/(kT_e). \quad (2)$$

The electron temperature can therefore be calculated directly from the I-V characteristic of the probe. Deviations from linearity in the plot of $\ln i_e$ vs V_p are a result of non-Maxwellian electron distributions. For $V_p \ll 0$, the current collected is totally due to positive ions. For $V_p \gg 0$, and in the absence of negative ions, the current collected is due totally to electrons and is nearly constant. From this current, called the electron-saturation current i_{e0}, the electron density can be calculated from the relationship

$$i_{e0} \approx -\tfrac{1}{4} n_0 e [(8kT_e)/(\pi m_e)]^{1/2}. \quad (3)$$

[a)]Present address: Lawrence Livermore National Laboratory, University of California, MS-L467, Livermore, CA 94550.

 0021/8979/82/042939-08$02.40

Several problems arise when making probe measurements in an rf plasma. The source of this difficulty is that an rf voltage will form across the plasma-probe junction. The *I-V* characteristic of the probe, which is an average over many millions of rf cycles, can be distorted by this ac component.[18] For example, assuming that the collection of electron current is exponential with respect to the probe voltage, the instantaneous probe current is

$$i_e(t) = i_{e0} \exp[(-e/kT_e)(V_{dc} + V_{ac} \sin \omega t - Ri_e(t))], \quad (4)$$

where the probe voltage is expressed as the sum of the applied dc bias and an ac component, T_e is the electron temperature and R is an ohmic voltage drop across the sheath. Averaging (4) over an rf cycle, and ignoring R for the moment,

$$\bar{i}_e = i_{e0} \exp[-(e/kT_e)(V_{dc} + \Delta V)], \quad (5)$$

where $\Delta V = (-kT_e/e) \ln [\mathcal{J}_0(-eV_{ac}/kT_e)]$, and $\mathcal{J}_0$ is the modified Bessel function of the first kind. The result of the averaging process is to impose a dc shift in the *I-V* characteristic of the probe with respect to the applied bias. The shift alone does not perturb the shape of the characteristic. The ohmic term in (5), though, can distort the upper part of the *I-V* characteristic as well as decrease the magnitude of the dc shift. The electron temperature one calculates from the slope of the *I-V* characteristic is accurate provided the distorted region is not used. The dc shift of a typical probe *I-V* characteristic is shown in Fig. 1.

The distortion of the *I-V* characteristic is especially important when attempting to calculate the electron-flux distribution from the *I-V* characteristic. It can be shown that the second derivative of the probe current with respect to the probe bias is proportional to the flux distribution.[24] That is

$$f(\epsilon) = \frac{4}{Aen_0}\left(\frac{m_e V_p}{2e}\right)^{1/2} \left.\frac{d^2 i(V_p)}{dV_p^2}\right|_{eV_p = \epsilon}, \quad (6)$$

where m_e is the electron mass, e is the electron charge, A is the probe area and $f(\epsilon)$ is the flux distribution. (At pressures where the mean-free-path of the electron is comparable to the probe radius, there is an additional correction term to (6).[26] In this discussion, that correction is not applicable.) The distortion of the *I-V* characteristic in the upper part of the curve (where $V_p \simeq 0$) results in an error in $f(\epsilon)$ for small ϵ. For conditions of interest here, the error is for ϵ less than about 3 to 5 eV. The difficulty in determining precisely where $V_p = 0$ may also lead to an offset in $f(\epsilon)$ on the ϵ axis of a few electron volts.

To minimize errors in the interpretation of probe data taken in rf plasmas, one should limit the parameter space for any given set of measurements so that the distortion of the *I-V* characteristic is consistent for all cases. The absolute values of the measurements may be suspect, but the relative values should be reliable. This limitation means that the rf power (i.e., E_{ac}/P) should be kept nearly constant. In view of the difficulties in interpreting the probe data, for a given set of data in this study the rf power was kept constant. Since the coupling of the rf supply to the discharge depends, in part, on the composition of the gas (this being one of the variables),

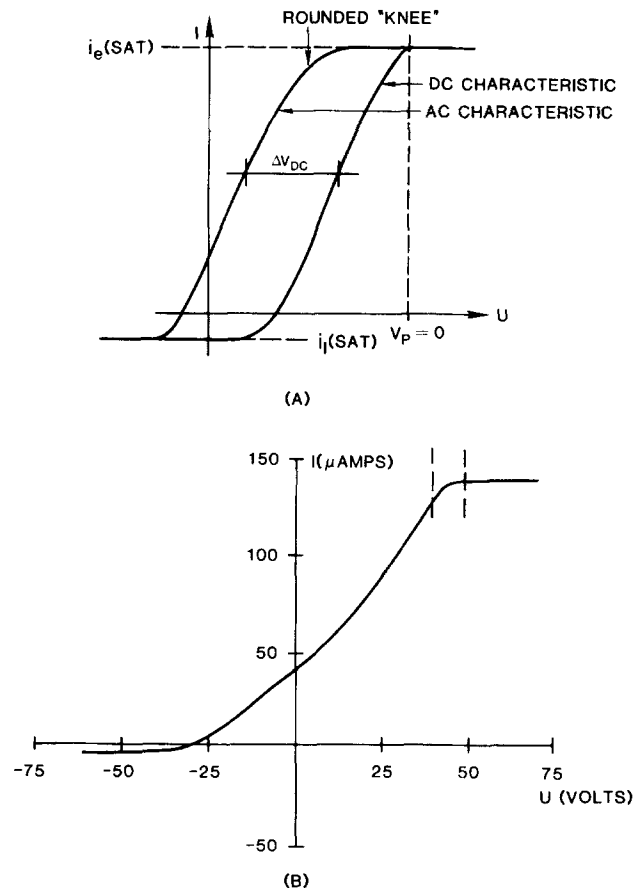

FIG. 1. (a) Schematic of probe *I-V* characteristics in dc and ac discharges. Note the offset in the ac characteristic and the rf distortion (the "rounded knee"). (b) Typical probe *I-V* characteristic for an rf discharge in 85 m Torr of CF_4 (680 V peak-to-peak). The distorted region is between the dotted lines.

the impedance-matching network was tuned off of the optimum settings for coupling power into the gas. It was found that, with this arrangement, the rf E/P and power deposited in the gas were relatively insensitive to the gas composition.

Plasma-etching discharges typically have a large mole fraction of electron-attaching species and therefore have a large density of negative ions. It can be shown that, for a large positive bias on a probe, the ratio of the contribution to the current of negative ions with respect to electrons is

$$\frac{i_I}{i_e} = \left(\frac{n_I}{n_e + n_I}\right)\left(\frac{m_e T_I}{m_I T_e}\right)^{1/2}. \quad (7)$$

In Eq. (7), the subscripts I and e refer to ions and electrons, respectively, and i is the current, n is the density, m is the particle mass, and T is the temperature. For the conditions of interest here, the minimum mass of a negative ion which might have a significant density is 19 amu (F^-), and the ratio of ion density to electron density is at most 1.[13] Therefore $i_I/i_e \simeq 6 \times 10^{-3} (T_I/T_e)^{1/2}$. Since $T_e \gg T_I$, the contribution of negative ions to the electron-saturation current is negligible.

III. EXPERIMENTAL ARRANGEMENT

The experimental setup for making the probe measurements is shown in Fig. 2. The plasma-etching reactor consisted of a pair of parallel plates 40 cm in diameter, separated

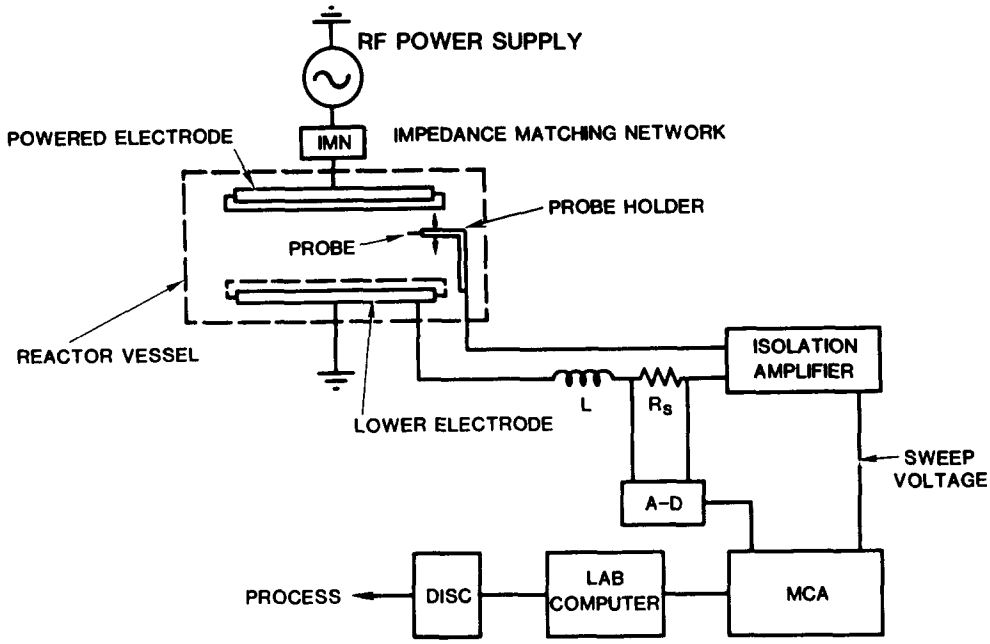

FIG. 2. Schematic of the experimental apparatus. The probe was mounted on a translator in order to change its height in the reactor. The plasma-etching reactor vacuum wall was a pyrex ring.

by 3 cm. An impedance-matching network interfaced the reactor to a 1 kW, 13.56 MHz rf power supply. The input gases were metered by digital-readout flow meters and evacuated from the chamber by a turbomolecular pump. The pumping speed of the turbomolecular pump varied with the composition of the gas. Therefore, to keep total flow rates (in sccm) and the reactor pressure constant as the composition of the gas was changed, the throttle of the pump had to be adjusted.

The Langmuir probe was made of 5-mil tungsten wire, 4–5 mm in length. Data was collected on a Tracor Northern 1710-multichannel analyzer. The sweep output of the MCA, isolated and amplified, was used to bias the probe. The signal collected from a sensing resistor in the probe circuit was amplified and digitized by the MCA where it was stored. The *I-V* characteristic, which was the average of 20 to 50 sweeps, was finally dumped to a laboratory computer for processing. The time required for a single sweep, approximately 5 s, was sufficiently long so that the measurements at any given probe bias can be considered dc values. Negative ions are therefore also collected, although their contribution is small.

The powered (upper) electrode was covered by an anodized aluminum plate, which made it an effectively insulated surface. The lower electrode was grounded and was either bare aluminum or partially covered by an anodized aluminum plate. In the instances where the lower electrode was partially covered, the bare electrode was sufficiently exposed to complete the probe circuit.

To insure that the probe was not fouled by polymer formation during the experiment, thereby changing the effective probe area, the following procedures were followed. Data was taken on different days while randomly changing the parametric variable. In this way, cummulative fouling of the probe could be detected by significant changes in the results. In addition, the bias on the probe was occasionally and momentarily made sufficiently large so that the tungsten wire would begin to glow. In this way, any polymer formed on the surface of the probe would be sputtered or boiled off.

IV. EXPERIMENTAL RESULTS

Mixtures of C_nF_m/H_2 and C_nF_m/O_2 (e.g., $C_nF_m = (CF_4, C_2F_6)$ are often used in plasma-etching discharges to increase or decrease the selectivity of etching one particular surface with respect to another.[2] Mixtures of C_nF_m/H_2 increase the selectivity of SiO_2 with respect to Si, while C_nF_m/O_2 mixtures increase the selectivity of etching Si with respect to SiO_2. The change in electron density which occurs as the gas mixture is varied in this manner was measured in our reactor.

Results from the Langmuir probe measurements show a decrease in electron density as the CF_4/H_2 mixture is varied from all CF_4 to all H_2 (see Fig. 3). The decrease is not monotonic, as a local maximum in electron density occurs near a CF_4/H_2 ratio of 0.4/0.6. Also plotted in Fig. 3 is the calculated electron density using the model described in Ref. 13. The calculation also shows a decrease in electron density as the CF_4/H_2 ratio decreases, but it fails to reproduce the local extrema in density. The possible reasons for failing to reproduce the local extrema will be discussed below.

At large E/P (>40 V/cm Torr) the drift velocity of electrons in CF_4 and H_2 are comparable. At $E/P = 70$ V/cm Torr, the drift velocity in hydrogen is 3×10^7 cm/s with a slope of 4.9×10^5 Torr cm^2/V s.[27] In CF_4, these values are 2.2×10^7 cm/s and 4.3×10^5 Torr cm^2/V s.[28] The ionization coefficients in CF_4 and H_2 are also comparable at moderate E/P. However, in hydrogen, the ionization coefficient saturates and is nearly constant at about $\alpha/P = 4$ V/cm Torr for $E/P > 400$ V/cm Torr.[29] Data ia not available for α in the range of $E/P > 400$ V/cm Torr in CF_4. Similar molecules, though, do not exhibit the saturation in α as does hydrogen. The ionization potential of H_2 is 15.6 eV while that of CF_4 is 13.6 eV (which is the appearance potential of CF_3^+ from CF_4). Therefore, despite the fact that the rf breakdown voltage was found to be significantly larger for CF_4 than for H_2, one may expect the electron density at high E/P to be comparable in the two gases and, for sufficiently

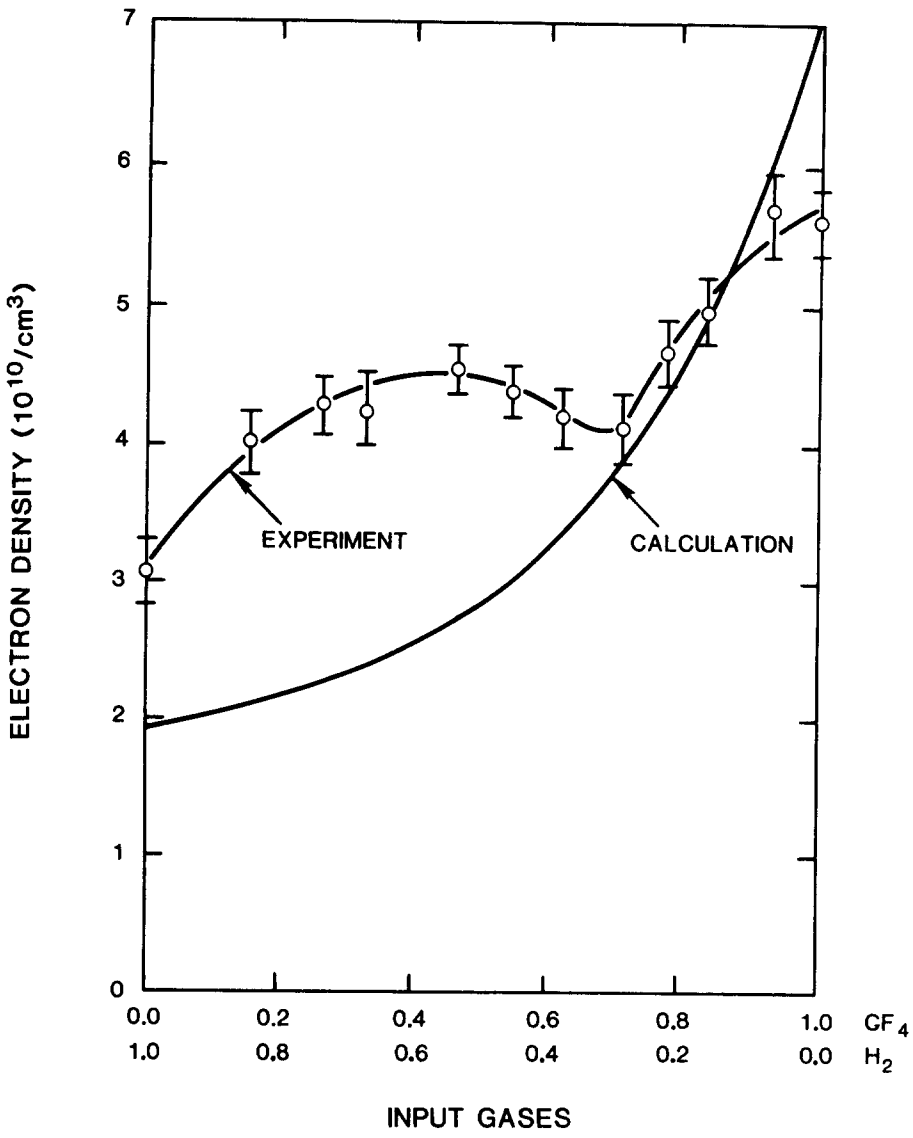

FIG. 3. Electron densities in CF_4/H_2 discharges. Total pressure (97 m Torr) and flow rate (95 sccm) were held constant. The peak-to-peak rf voltage was 640 V. The calculation was normalized to the experimental data.

high E/P, to be larger in CF_4. The requirement on E/P for this to occur is that the average electron energy be sufficiently high so that the resonant, low-energy electron-impact events (e.g., vibrational excitation, dissociative attachment) are no longer important (see discussion below).

Similar results are obtained for measurements of electron densities in CF_4/O_2 mixtures. Experimental and computed results are shown in Fig. 4. Again we see a decrease in electron density as the mixture changes from all CF_4 to all oxygen, with a local maximum in density near a CF_4/O_2 ratio of 0.3/0.7. The computed results reproduce the decrease in electron density but fail to show an extrema.

The failure of the computed results to reproduce the observed extrema in electron density is an artifact of the model.[13] The steady-state electron density for a given gas mixture was calculated as a function of the rf power deposited in the gas:

$$n_e = \frac{P}{\sum_{i,j} r_{ij}[N_i]}, \tag{8}$$

where n_e is the steady-state electron density, P is the power deposited in the gas per unit volume, r_{ij} is the rate at which electrons lose energy to species i by collision process j, and $[N_i]$ is the density of species i. The electron density and distribution function were calculated on the basis of the input gases and therefore ignore secondary and intermediate species which could effect the outcome of the calculation.

When changing the gas mixture in CF_4/O_2 and CF_4/H_2 discharges to large concentrations of CF_4, a structure develops in the experimentally measured flux distribution. This is illustrated in Fig. 5, where the measured flux distribution is plotted for three separate CF_4/O_2 mixtures. Similar behavior is observed for CF_4/H_2 mixtures. The space potential (i.e., where $V_p = 0$) was established by the point at which $d^2I/dV^2 = 0$ (see Fig. 1). The measured curvature of $f(\epsilon)$ is positive for small ϵ whereas a Maxwellian or Dryvestyn distribution start with negative curvature. This discrepancy may be a result of the previously mentioned rf distortion of the I-V characteristic near $V_p = 0$. This anomalous curvature has also been seen in high E/P microwaves discharges in nitrogen.[17] The structure in $f(\epsilon)$ for $\epsilon > 20$ eV is qualitative, but similar structure has been observed by other investigators in discharges in N_2, [17,30] and Ne-H_2.[31] The origin of this structure in a high E/P rf discharge might be explained as follows.

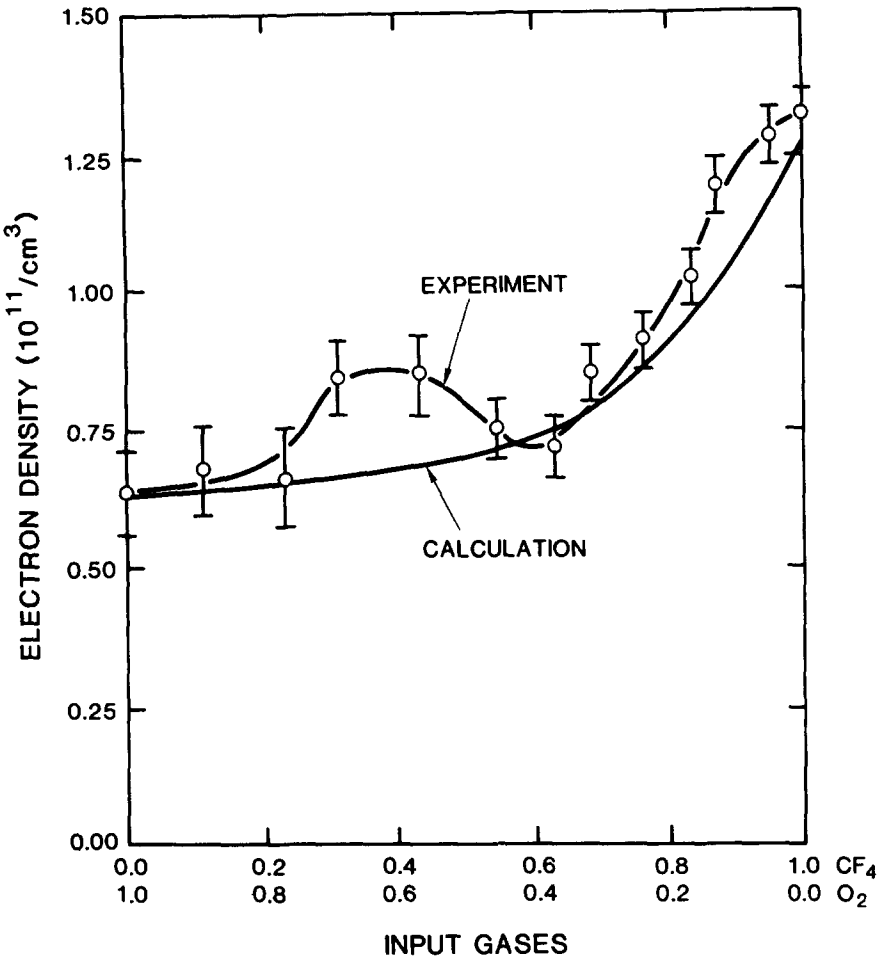

FIG. 4. Electron densities in CF_4/O_2 discharges. Total pressure (85 m Torr) and flow rate (100 sccm) were hold constant. The peak-to-peak rf voltage was 680 V. The calculation was normalized to the experimental data.

If the range of electron energy over which inelastic processes are important changes as the gas composition is varied, then one would expect that $f(\epsilon)$ would change. The change in $f(\epsilon)$ observed as the fraction of CF_4 increases suggests that in CF_4, once electrons are accelerated beyond an energy where resonant types of excitations may be expected to occur, there are fewer processes to slow the electrons down. Therefore a large, high-energy electron flux is possi-

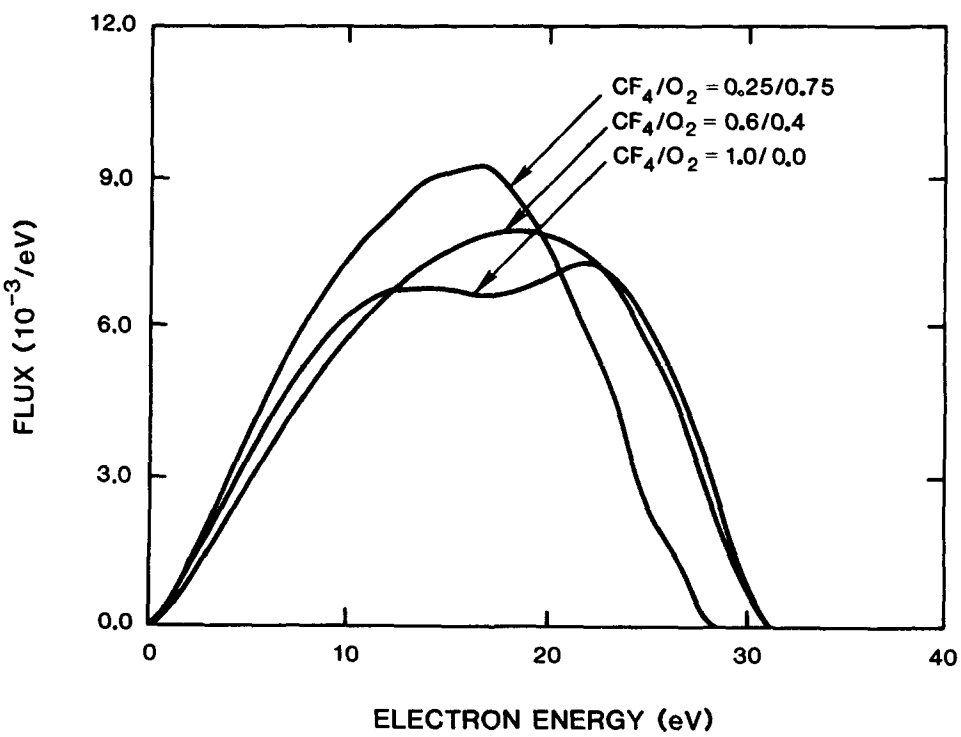

FIG. 5. Electron flux distributions calculated from experimental *I-V* characteristics for various CF_4/O_2 gas mixes. The conditions are the same as for Fig. 4. Note the shift in the maximum flux to higher electron energy as the fraction of CF_4 is increased.

ble. Dissociation products may also contribute to large inelastic collision rates at low ϵ. For conditions where the applied E/P is too small to breach the resonant region, or the gas has cross sections with more typical nonresonant cross sections, one would not expect to see this structure.

Another contributing factor to the observed structure is the oscillating rf field. Remember that probe measurements at a given bias are an average over many thousands of rf cycles. During a given cycle, the applied voltage can change by many hundreds of volts. If one assumes that the flux distribution tracks the applied electric field, then during one cycle, the instantaneous flux distribution will change dramatically. This is illustrated in Fig. 6, where the calculated flux distribution for an ideal CF_4 discharge is plotted for many different values of E/P during a single rf cycle.[13] When averaging these distributions, the result can have an extrema occurring at large ϵ.

One of the assumptions made in probe theory is that the plasma is homogeneous and large in dimensions compared to the mean-free-path of an electron. In the low-pressure (< 100 m Torr) hot plasmas investigated here, that assumption is not always valid. The mean-free-path of a 10-eV electron in a gas at 50 m Torr pressure is about a centimeter, while the transverse dimension of the reactor is 3 cm. This situation has three consequences. First, diffusion may not be a good description of the transport of electrons. Second, comparing probe measurements made at different locations in the reactor may be suspect. Third, boundary conditions imposed by the electrode surfaces will greatly influence the properties of the plasma.

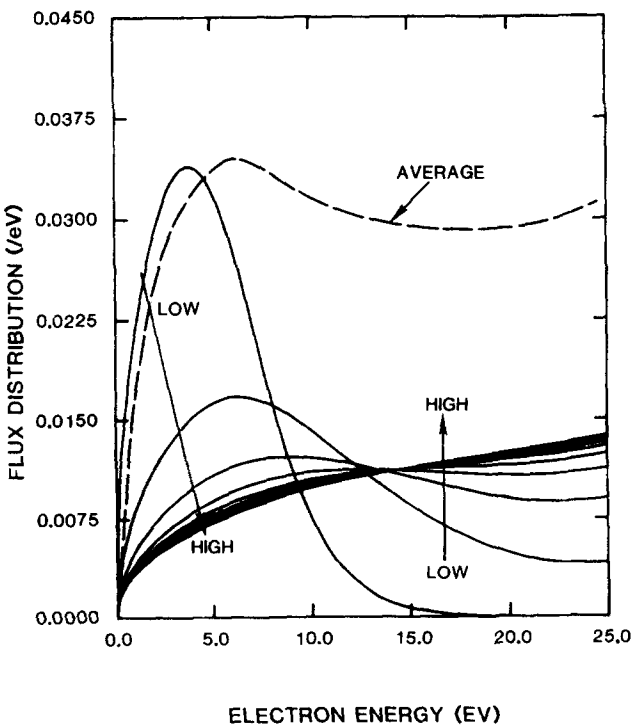

FIG. 6. Calculated flux distributions for various E/P in a 100 m Torr, 750 V peak-to-peak CF_4 discharge. The arrows point in the direction of increasing E/P. The average (renormalized) of the instantaneous flux distributions can result in a distribution with an extrema at large electron energies.

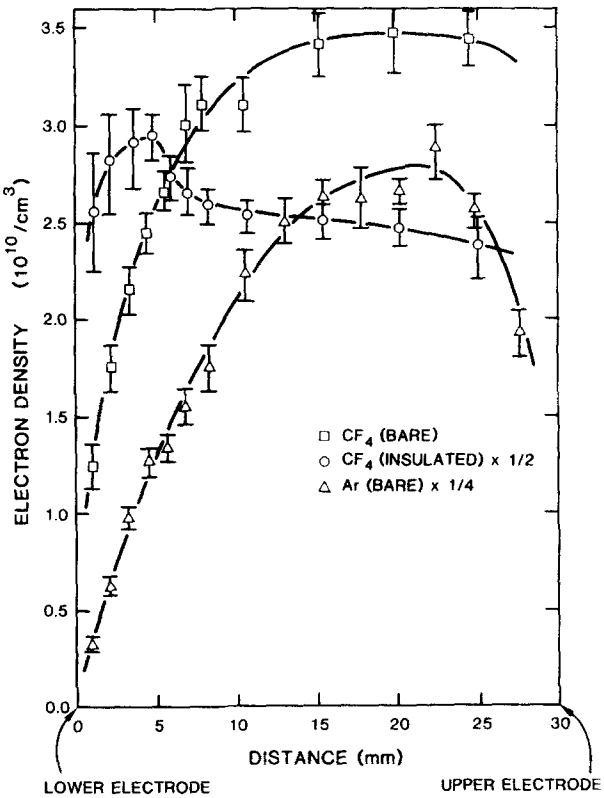

FIG. 7. Electron densities in a CF_4 discharge (22 m Torr, 590 V peak-to-peak) as a function of distance between the electrodes for bare (■) and insulated (●) lower electrode. For comparison, a similar measurement in argon (80 m Torr 280 V peak-to-peak) is also plotted.

Understanding the consequences above, it is of interest to examine measurements of electron density as a function of position between the electrode plates in our plasma-etching reactor. In Fig. 7, electron densities in a CF_4 plasma with both a conducting and an insulated lower electrode are plotted. (Recall that the upper-powered electrode is insulated.) Typical I-V characteristics are shown in Fig. 8. In the asymmetric case, the conducting surface has a smaller dc component (if any) to its sheath potential than does an insulated surface. This, in turn, decreases the local space-charge field. Large space-charge fields near a surface in a sense protect the plasma from that surface by turning back or slowing down electrons which might otherwise reach the surface and recombine. The net result is that the electron density is small near the conducting electrode and increases to a near constant value in the body of the plasma. There is a decrease in density as the powered, insulated electrode is approached, but the decrease is smaller. Similar behavior is observed for other gases (e.g., Ar, C_2F_6).

In the case where both electrodes are insulated, the asymmetry discussed above no longer exists, and the electron density is nearly uniform. Both electrodes have large dc components to the sheath potential. In this example, the mean-free-path of the electron is long enough so that classic ambipolar diffusion does not yet apply. As the gas pressure increases and the mean-free-path decreases, diffusion becomes a more appropriate description. Near the lower electrode, there appears to be a local increase in electron density. This was observed under a variety of conditions, and can be

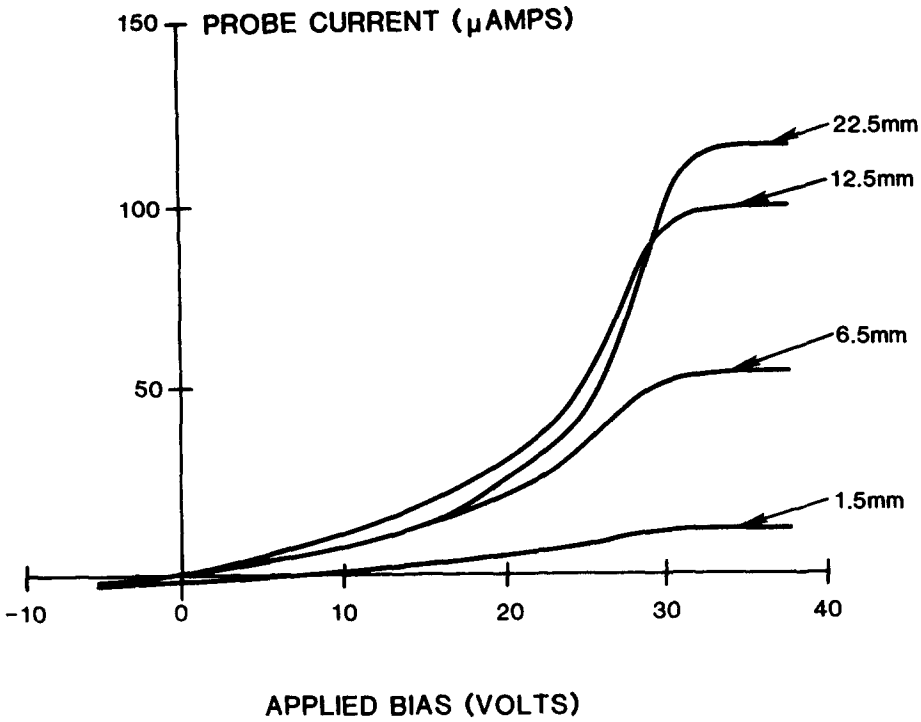

FIG. 8. I-V characteristics for a discharge in argon as a function of height above the lower (bare) electrode.

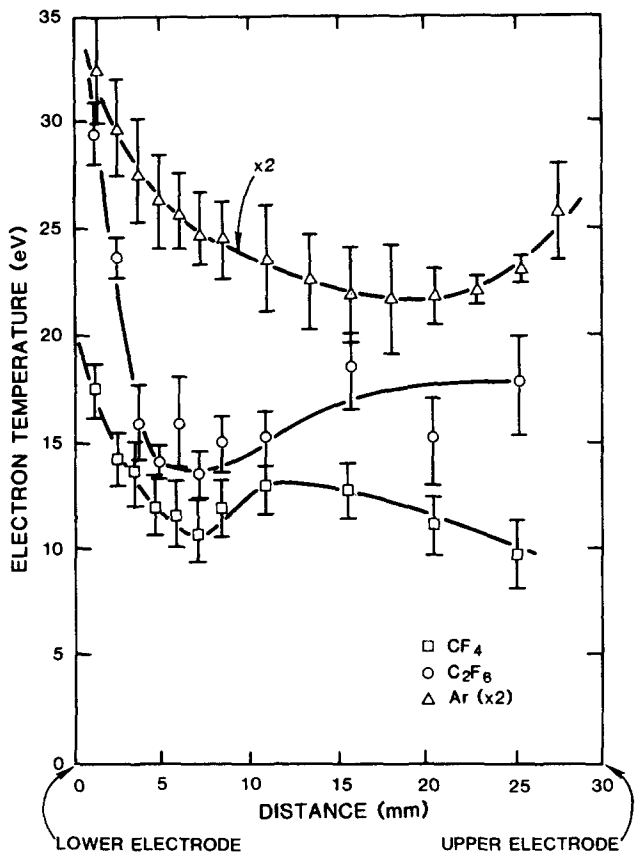

FIG. 9. Electron temperature as a function of distance between the probe and the lower electrode for discharges in CF_4, C_2F_6 and Ar. Discharge conditions for CF_4 and C_2F_6 are 22 m Torr pressure and 590 V peak-to-peak rf voltage. For Ar the conditions are 80 m Torr and 280 V. In all cases, the electron temperature increases near the lower, bare electrode. There appears to be no systematic change in electron temperature near the upper-powered insulated electrode.

qualitatively explained by the sheath potential which forms a barrier to electrons which are accelerated toward the wall.

The electron temperature is also a function of position in the reactor, examples of which are plotted in Fig. 9. The electron temperature is a qualitative number since the plasma is non-Maxwellian, and the ln (i_e)-V plot is not a straight line. Nevertheless, an average electron temperature can be assigned. The error bars in Fig. 9 represent the range of the electron temperature which one could calculate from different portions of the ln (i_e)-V plot. The smaller the error bar, the more nearly Maxwellian the plasma is. This variation in the electron temperature results in a range of calculated electron density since $n_e \sim T_e^{-1/2}$. In all cases, the electron temperature increases near the bare electrode and decreases near the center of the reactor. The electron temperature would appear to increase near the powered, insulated electrode; however, the precise behavior is a function of the type of gas.

To study in more detail electron properties in parallel plate rf discharges, a classical Monte Carlo computer code has been written. Results from that code provide some insight to the conditions required in order for the electron temperature to have the observed profiles. The oscillatory electric field in the plasma must be small ($E \lesssim 10$ V/cm), and the secondary emission coefficient for electrons by ions accelerated into the electrodes by the sheath potential must be large ($\gamma \gg 0.1$). Energetic electrons are provided by secondary electrons which accelerate down the sheath potential into the plasma.

V. CONCLUDING REMARKS

Plasma-etching discharges are especially complex systems due to their large E/P, nontraditional gases, and the concurrent neutral chemistry which may occur. Under con-

ditions of interest for plasma etching, we have seen that electron temperatures ($T_e \gtrsim 15$ eV) and densities ($n_e \gtrsim 10^{11}/\text{cm}^3$) can be large. The particular materials of the electrode surfaces can greatly influence the distribution of electrons in the reactor, especially when the mean-free-path of the electron is comparable to the electrode separation.

ACKNOWLEDGMENT

This work was supported by the Department of Energy.

[1]J. Hayes and T. Pandhumsoporn, Solid State Technol. **11**, 71 (1980).
[2]J. W. Coburn and E. Kay, IBM Res. Dev. **23**, 33 (1979).
[3]J. W. Coburn and H. F. Winters, J. Vac. Sci. Technol. **16**, 391 (1979).
[4]B. Chapman, *Glow Discharge Processes* (Wiley, New York, 1980).
[5]E. A. Truesdale, G. Smolinsky, and T. M. Mayer, J. Appl. Phys. **51**, 2909 (1980).
[6]E. A. Truesdale and G. Smolinsky, J. Appl. Phys. **50**, 6594 (1979).
[7]B. A. Raby, J. Vac. Sci. Technol. **15**, 205 (1978).
[8]C. J. Mogab, A. C. Adams, and D. L. Flamm, J. Appl. Phys. **49**, 3796 (1978).
[9]R. G. Frieser and J. Nogay, Applied Spectrosc. **34**, 31 (1980).
[10]W. R. Harshbarger, R. A. Porter, T. A. Hiller, and P. Horton, Appl. Spectrosc. **31**, 201 (1977).
[11]D. L. Flamm, J. Appl. Phys. **51**, 5688 (1980).
[12]H. F. Winters, J. W. Coburn, and E. Kay, J. Appl. Phys. **48**, 4973 (1973).
[13]M. J. Kushner, J. Appl. Phys. **53**, 2923 (1982).
[14]V. N. Babichev, V. A. Zavadskii, and D. V. Orlinskii, Sov. J. Plasma Phys. **3**, 750 (1977).
[15]V. A. Godyak and O. A. Popov, Sov. Phys. Tech. Phys. **22**, 461 (1977).
[16]Yu. A. Ivanov, Yu. A. Lebedev, and L. S. Polak, Sov. Phys. Tech. Phys. **21**, 830 (1976).
[17]V. F. Babel'yanta, F. B. Vurzel, and L. S. Polak, Sov. Phys. Tech. Phys. **18**, 1197 (1974).
[18]A. Cantin and R. R. J. Gagne, *Third International Conference on Gas Discharges*, London, 1974, pp. 625–9.
[19]R. R. J. Gagne and A. Cantin, J. Appl. Phys. **43**, 2639 (1972).
[20]J. A. Thornton, J. Vac. Sci. Technol. **15**, 188 (1978).
[21]E. Eser, R. E. Ogilvie, and K. A. Taylor, J. Vac. Sci. Technol. **15**, 199 (1978).
[22]S. M. Ojha, Vacuum **27**, 65 (1977).
[23]H. Norstrom, R. Olaison, S. Berg, and L. P. Anderson, J. Electrochem. Soc. **127**, 2680 (1980).
[24]L. Schott, in *Plasma Diagnostics*, edited by W. Lochte-Holtgreven (North Holland, Amsterdam, 1968), pp. 668–731.
[25]F. F. Chen, in *Plasma Diagnostic Techniques*, edited by R. H. Huddlestone and S. L. Leonard (Academic, New York, 1965), pp. 113–200.
[26]S. D. Vagner and B. K. Ignat'ev, Sov. Phys. Tech. Phys. **22**, 558 (1977).
[27]H. A. Blevin, J. Fletcher, and S. R. Hunter, J. Phys. D **9**, 1671 (1976).
[28]M. S. Naidu and A. N. Prasad, J. Phys. D **5**, 983 (1972).
[29]S. C. Brown, *Basic Data of Plasma Physics* (MIT, Cambridge, Mass., 1959).
[30]J. D. Swift, Brit. J. Appl. Phys. **16**, 837 (1965).
[31]V. L. Afanas'eva, A. V. Lukin, and K. S. Mustafin, Sov. Phys. Tech. Phys. **12**, 233 (1967).